scientific reports

Check for updates

OPEN

Modified Green-Ampt model for infiltration analysis in loess area and its parameter determination and verification

Yunxin Zheng[1], Zhiping Hu[1]✉, Rui Wang[1], Songli Chen[1], Xiang Ren[2] & Yonghui Zhang[1]

Water infiltration into soil is important in geotechnical engineering. The classical Green-Ampt (GA) infiltration model is widely used in soil infiltration due to its physical significance, but it ignores the actual unsaturated layer in the infiltration process and has some deficiencies. Thus, the present study established a modified GA infiltration model (MLGA model) using Darcy's infiltration law and continuity equation to fully consider the variation characteristics of the soil water profile in the infiltration process. The Philip model and the GA model have the same physical basis. By combining the internal relationship between the infiltration rate and cumulative infiltration of the two models, the expression of matrix suction of the MLGA model was obtained. The existing measured data was used to verify the correctness and applicability of the MLGA model. Finally, the sensitivity analysis of the critical parameters of the model was performed. The results showed that the MLGA model is reliable and can be used for water infiltration analysis in loess sites. When the MLGA model is used to calculate the infiltration depth, the maximum relative error between the calculated value and the measured data is less than 10%, and the average relative error is 5.54%, which indicates that the model has a high calculation accuracy. The average error of the MLGA model is 24.47% of the Kostiakov model and 80.42% of the existing modified GA model (LGAM model). Sensitivity analysis of the saturated permeability coefficient, initial water content, saturated water content, and matrix suction was performed using the single-factor disturbance method. The influence of each parameter on infiltration depth was summarized, and the sensitivity of each parameter was quantitatively evaluated, which revealed that saturated water content is a highly sensitive parameter. When using the MLGA model to calculate infiltration depth, the accuracy of saturated water content should be ensured first. Finally, the difference between the MLGA model and the LGAM model in describing the whole process of water infiltration is discussed, and the influence mechanism of critical parameters on the water infiltration process is deeply analyzed. The established MLGA model provides theoretical support for further study of the loess water infiltration mechanism.

Keywords Loess, Infiltration, Green-Ampt model, Cumulative infiltration, Wetting front depth

Loess, as a Quaternary sediment, is widely distributed in semi-arid and arid areas, accounting for approximately 10% of the global land area[1–3]. China has the most extensive loess deposit in the world, distributed in a band in China (Fig. 1), covering an area of approximately 631,000 km^2[4]. In recent years, with China's "One Belt, One Road" initiative and the Western Development Strategy, infrastructure construction in the loess area has increased[5]. The unique water sensitivity of loess gives rises to engineering problems, such as pavement collapse and uneven settlement of buildings after water infiltration (Fig. 2), which poses a severe threat to the service state of road engineering and the safety and stability of existing buildings and structures[6–9]. To effectively prevent and solve these problems, it is necessary to establish a water infiltration model suitable for loess sites and to explore the law of water infiltration in loess foundations, which has important practical significance.

Currently, the existing infiltration models are mainly divided into two categories, namely empirical and physical models[10,11]. Empirical models, such as the Kostiakov model and Horton model, have simple expressions and a quick and easy computational process[12]. In general, the calculation accuracy of empirical models is highly dependent on determining model parameters. However, the parameters of empirical models cannot be directly

[1]School of Civil Engineering, Chang'an University, Xi'an 710061, China. [2]School of Civil Engineering, Shandong University of Aeronautics, Binzhou 256600, China. ✉email: huzhping@chd.edu.cn

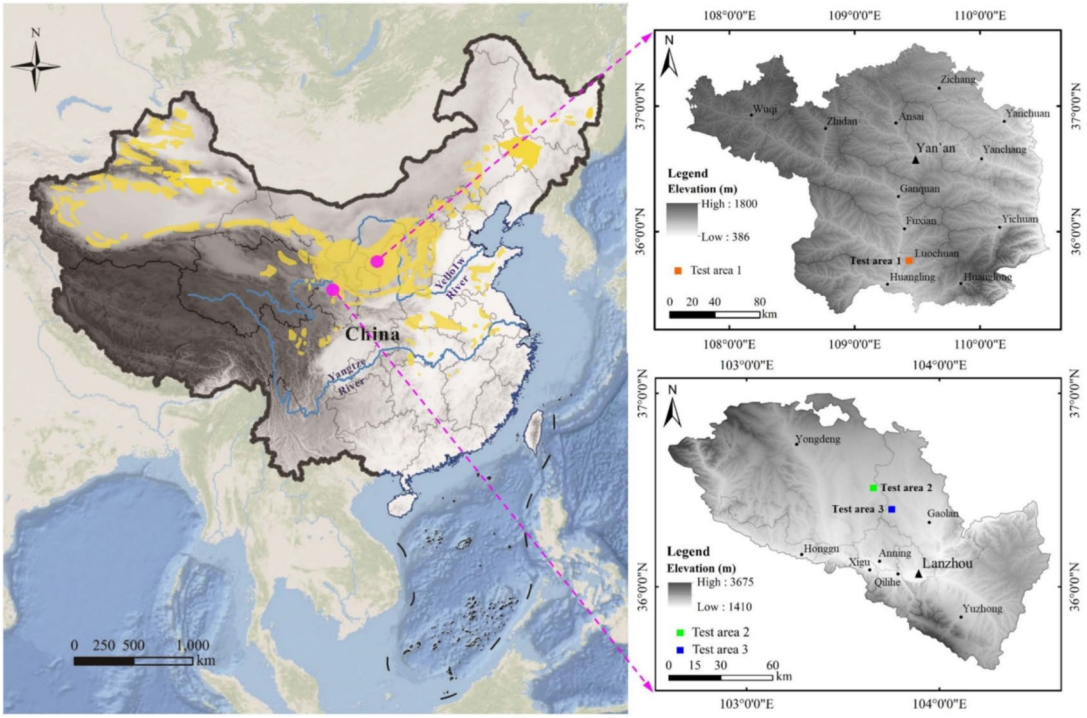

Fig. 1. Distribution of loess in China and test areas. (This figure was created by the authors using ArcGIS software version 10.8, http://www.ersi.com/)

Fig. 2. Typical engineering issues in loess areas.

obtained by soil parameters and need to be fitted based on field or indoor measured data. Therefore, the process of model parameter determination is subjective, and some human errors may be introduced in the model calculation process. Further, the model parameters do not have a clear physical meaning.

Physical models, which are based on Darcy's law and the water balance principle, describe the infiltration process by a differential equation[13]. Richard's equation and the Green-Ampt (GA) model are the most widely used physical models[14,15]. Richard's equation has a strict physical basis and is often used as a partial differential equation to study the water movement in soil with high calculation accuracy. However, due to the strong nonlinearity of Richard's equation, the calculation process is cumbersome, and it is difficult to obtain an accurate analytical solution[16]. The GA model, also known as the piston model, is proposed by Green and Ampt based on the capillary theory, which describes the infiltration process of the initial uniform dry soil under the condition of thin layer water accumulation. The GA model is simple, and the parameters are easy to obtain[17,18]. Moreover, the GA model has strong universality and can be solved by a simple analytical method[19]. Therefore, the GA model has attracted much attention and is widely used in engineering practice[20,21]. Mein and Larson[22] and Chu[23] improved the classical GA model by studying the relationship between rainfall intensity and infiltration rate. Considering the influence of slope and initial water content, Cho[24], Yao et al.[25], and Liu et al.[26] established modified GA models. Dou et al.[27] established a rainwater infiltration redistribution analysis model based on the GA infiltration model to take into account the variability of soil saturation permeability coefficient. Ma et al.[28] modified the GA model by introducing the concept of saturation coefficient and developed a GA model suitable for layered soils. Tsai et al.[29] conducted infiltration tests using sandy soils with different grain sizes and proposed a dynamic effect infiltration model considering capillary pressure. Kang et al.[30] established a muddy water infiltration model based on the GA model. Zha et al.[31] developed a modified GA model to reflect the variation characteristics of the wetting front, and they validated the modified model with experimental data.

The abovementioned modified models follow the basic assumptions of the GA model and have achieved a series of important results, promoting the development of infiltration models. On the basis of the summary and analysis of many indoor tests and measured infiltration data, scholars have found that the soil in the infiltration depth is not completely saturated and that part of the soil is unsaturated. Therefore, the soil in the infiltration depth is considered to be saturated, which is inconsistent with the actual situation, thus resulting in certain deficiencies.

In studies of water infiltration in loess areas, Wang et al.[32], Peng et al.[33], and Wen et al.[34] first summarized the variation characteristics of the loess water profile during the infiltration process. According to different water contents in the infiltration depth, the soil layer is divided into a saturated layer and an unsaturated layer, allowing modified GA models suitable for loess area to be established. Although the existing established modified GA models for loess areas take into account the characteristics of the distribution of water content in the soil profile, the saturated layer depth at the initial infiltration stage is neglected in the model derivation process, which fails to reflect the actual dynamic water infiltration process thoroughly, resulting in certain shortcomings.

Based on existing research, the present study considered the actual dynamic infiltration process of water and the distribution characteristics of water content in the soil profile and established the a modified GA infiltration model (MLGA model) suitable for the water infiltration condition of loess areas. Using the internal relationship between the infiltration rate and the cumulative infiltration corresponding to the Philip model and the GA model, which have the same physical basis, the critical parameter of matrix suction of the MLGA model was derived. The effectiveness of the MLGA model was validated by comparison to three sets of high-quality published field infiltration test data and calculation results of existing models. Finally, the influence of critical parameters of the MLGA model on infiltration depth was explored by the single-factor disturbance method, and the sensitivity of each parameter was quantitatively described. Finally, the MLGA model and LGAM model were compared from the perspective of describing the whole process of water infiltration, and the influence mechanism of each critical parameter on the water infiltration process was deeply analyzed. The present results provide theoretical support for the study of water infiltration in loess areas, which is of great significance to the disaster prevention and mitigation of related construction projects in loess areas.

Infiltration model

Conventional GA infiltration model

The GA model is generally used to investigate the infiltration of dry soil in the presence of a thin layer of water[35–37]. The model assumes that there is a clear horizontal wetting front in the infiltration process, which divides the soil into the saturated area and dry area. The water content of the saturated area is saturated water content θ_s and the soil moisture content in the dry area is the initial moisture content θ_i[38,39]. Moreover, there is a fixed matrix suction s_f at the surface of the infiltration peak. Figure 3 shows a schematic diagram of GA model infiltration.

The GA model can be expressed as:

$$i = \frac{dI}{dt} = K_s \frac{z_f + h_0 + s_f}{z_f} \tag{1}$$

where i presents the infiltration rate; K_s presents the saturated water conductivity; z_f presents the wetting front depth; h_0 presents the thickness of the pounding water layer; and s_f is matrix suction.

The cumulative infiltration I can be expressed as follows:

$$I = (\theta_s - \theta_i)\, z_f \tag{2}$$

Combined with the law of conservation of mass and without ignoring the depth of surface water, the relationship between accumulated infiltration and infiltration time is as follows:

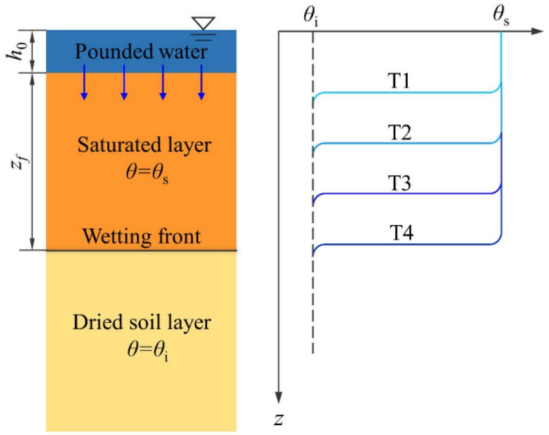

Fig. 3. Infiltration diagram of the GA model.

$$I = K_s t + (h_0 + s_f)(\theta_s - \theta_i) \ln [1 + I/(h_0 + s_f)(\theta_s - \theta_i)] \quad (3)$$

Proposed MLGA model

The classical GA model assumes that the wetting front is always a horizontal interface completely separated between dry and wet during the infiltration process, and the soil from the infiltration surface to the wetting front is completely saturated. However, previous studies have revealed a stratification phenomenon in the soil water profile within the wetting front infiltration depth, that is, there are simultaneous saturated and unsaturated layers. On the basis of field infiltration tests in loess areas, the depths of the saturated and unsaturated layers were approximately equal, suggesting that the classical GA model needs to be modified. The calculation schematic of the MLGA model applicable to the loess area in the present study is shown in Fig. 4.

The basic assumptions of the model are as follows: (1) During water infiltration, the soil layer within the infiltration depth is divided into the saturated layer and unsaturated layer ($L_1 = L_2 = 1/2L$);

(2) The water content of the saturated layer is saturated water content θ_s. The water content of the unsaturated layer changes with depth, and its distribution is reasonably characterized by the elliptic curve[40]. The horizontal semi-axis length of the elliptic curve is the difference between the saturated water content and the initial water content, and the longitudinal semi-axis length is the unsaturated layer thickness;

(3) Saturated layer infiltration flow is affected by pressure potential, gravity potential, and unsaturated layer suction potential gradient.

Based on the above basic assumptions, the cumulative infiltration I is written as:

$$\begin{aligned} I &= (\theta_s - \theta_i) L_1 + \frac{\pi}{4}(\theta_s - \theta_i) L_2 = (\theta_s - \theta_i)\frac{L}{2} + \frac{\pi}{4}(\theta_s - \theta_i)\frac{L}{2} \\ &= \frac{4+\pi}{4} L_1 (\theta_s - \theta_i) = \frac{4+\pi}{8} L (\theta_s - \theta_i) \end{aligned} \quad (4)$$

Then:

$$L = \frac{8I}{(4+\pi)(\theta_s - \theta_i)} \quad (5)$$

For the saturated layer, the infiltration rate i is expressed as follows:

$$i = \frac{dI}{dt} = K_s \frac{L_1 + h_0 + s_f}{L_1} = K_s \left[1 + \frac{(4+\pi)(\theta_s - \theta_i)(h_0 + s_f)}{4I}\right] \quad (6)$$

By integrating Eq. (6), the cumulative infiltration is expressed as:

$$I = K_s t + \frac{(4+\pi)(\theta_s - \theta_i)(h_0 + s_f)}{4} \ln \left[1 + \frac{4I}{(4+\pi)(\theta_s - \theta_i)(h_0 + s_f)}\right] \quad (7)$$

Because the Philip model has the same physical basis as the GA model[41,42], the correlation between the Philip model and the GA model was used to obtain the relevant parameters in the modified model.

In the Philip model, the specific expression for the infiltration rate i is as follows:

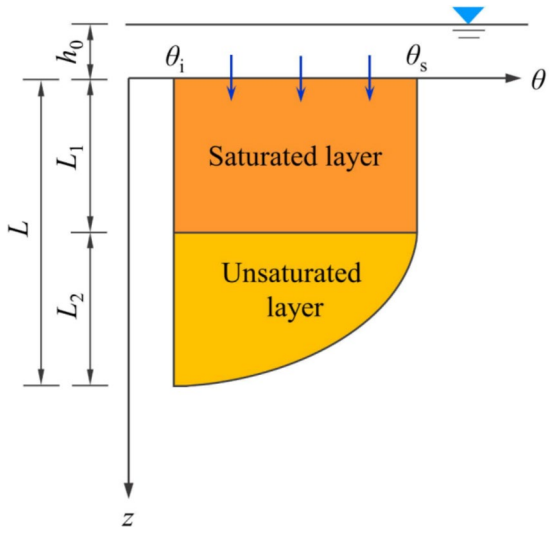

Fig. 4. Schematic illustration for the MLGA model.

$$i = \frac{1}{2}St^{-\frac{1}{2}} + A \tag{8}$$

where S is the infiltration rate of soil; and A is the steady infiltration rate.

Cumulative infiltration in the Philip model is calculated as:

$$I = St^{\frac{1}{2}} + At \tag{9}$$

At the initial stage of infiltration, matrix suction and water height play a significant role in the infiltration rate, allowing the Philip model to be simplified as follows:

$$i = \frac{1}{2}St^{-\frac{1}{2}} \tag{10}$$

$$I = St^{\frac{1}{2}} \tag{11}$$

In the GA model, the infiltration rate i is written as:

$$i = K_{\mathrm{s}}\frac{s_{\mathrm{f}} + h_0}{L_1} \tag{12}$$

Combining Eqs. (10) to (12) yields:

$$S^2 = \frac{(4+\pi)}{4}K_s\left(s_{\mathrm{f}} - h_0\right)\left(\theta_{\mathrm{s}} - \theta_{\mathrm{i}}\right) \tag{13}$$

From Eq. (13), the matrix suction s_{f} is expressed as follows:

$$s_{\mathrm{f}} = \frac{4S^2}{(4+\pi)\left(\theta_{\mathrm{s}} - \theta_{\mathrm{i}}\right)K_s} - h_0 \tag{14}$$

With the increase in infiltration time, the water infiltration rate in the soil is approximately equal to the saturated water conductivity of the soil, which indicates that the saturated water conductivity K_{s} in the GA model and A in the Philip model have the same physical significance, then:

$$K_{\mathrm{s}} = A \tag{15}$$

Further, Eq. (9) can be written as:

$$I = St^{\frac{1}{2}} + K_{\mathrm{s}}t \tag{16}$$

In the same infiltration time, the cumulative infiltration calculated by Eq. (7) and Eq. (16) should be equal, thus:

$$K_{\mathrm{s}}t + \frac{(4+\pi)\left(\theta_{\mathrm{s}} - \theta_{\mathrm{i}}\right)\left(h_0 + s_{\mathrm{f}}\right)}{4}\ln\left[1 + \frac{4I}{(4+\pi)\left(\theta_{\mathrm{s}} - \theta_{\mathrm{i}}\right)\left(h_0 + s_{\mathrm{f}}\right)}\right] = St^{\frac{1}{2}} + K_{\mathrm{s}}t \tag{17}$$

So,

$$I = \frac{(4+\pi)\left(s_{\mathrm{f}} + h_0\right)\left(\theta_{\mathrm{s}} - \theta_{\mathrm{i}}\right)}{4}\left[e^{\frac{4St^{\frac{1}{2}}}{(4+\pi)\left(s_{\mathrm{f}}+h_0\right)\left(\theta_{\mathrm{s}}-\theta_{\mathrm{i}}\right)}} - 1\right] \tag{18}$$

The combination of Eqs. (4), (13), and (18) gives the following equation:

$$L = 2\left(s_{\mathrm{f}} + h_0\right)\left[e^{\sqrt{\frac{4K_{\mathrm{s}}t}{(4+\pi)\left(s_{\mathrm{f}}+h_0\right)\left(\theta_{\mathrm{s}}-\theta_{\mathrm{i}}\right)}}} - 1\right] \tag{19}$$

As a conclusion, Eq. (19) is the expression of the MLGA model. Figure 5 shows the detailed computational steps of the MLGA model.

Model validation

The accuracy of the MLGA model was validated using measured data of loess areas reported by Wang et al.[32] and Liu et al.[43]. Moreover, the calculation results of the MLGA model were compared with those of the Kostiakov model and the existing modified GA model (LGAM model)[34]. The soil parameters and measured cumulative infiltration of each site are shown in Tables 1 and 2, respectively.

Considering test area No. 1 as an example, the matrix suction was calculated using the basic soil parameters. The soil absorption rate S was determined first. Inserting the measured cumulative infiltration and the corresponding infiltration time point into Eq. (11), $S = 0.50$ was obtained, and the goodness of fit was 97.36%

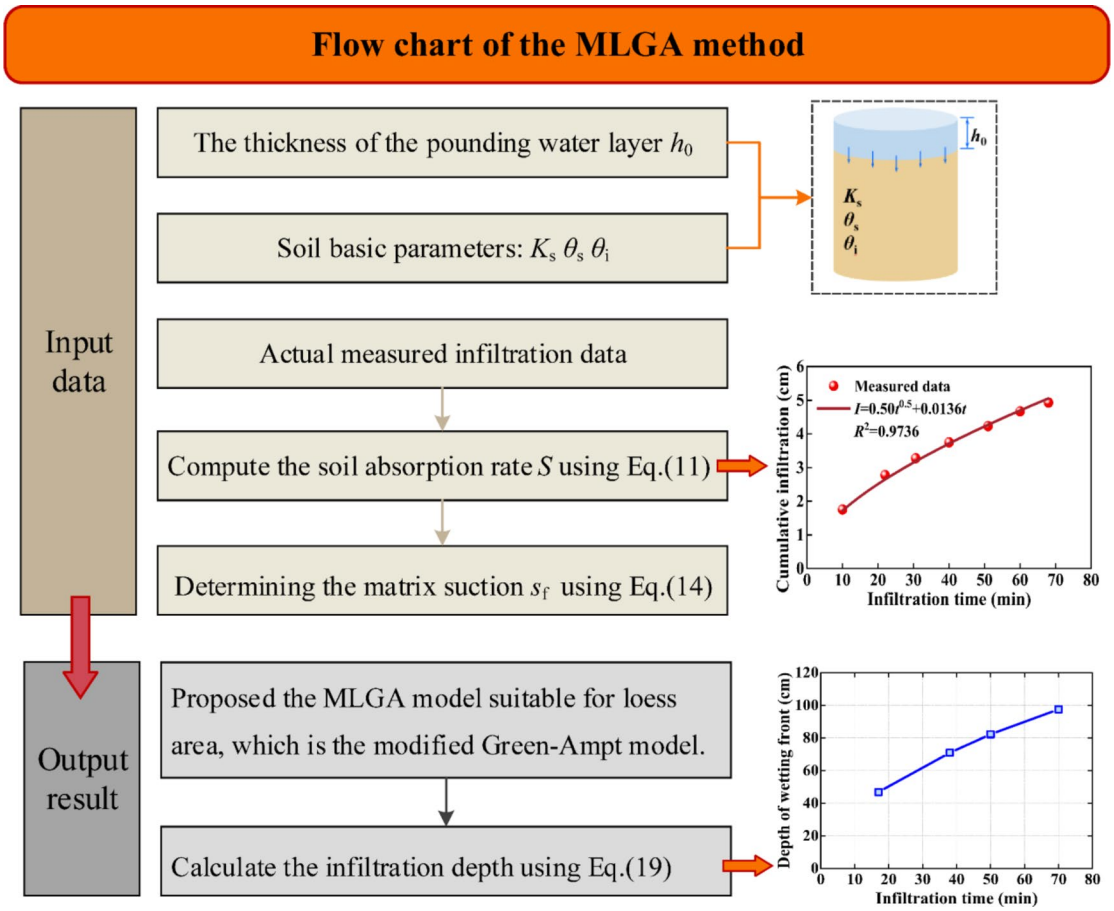

Fig. 5. Flow chart of the proposed MLGA model.

Area No.	Test area	Size of each grade (d/mm) ratio (%)			Initial water content θ_i (%)	Saturated water content θ_s (%)	Saturated permeability coefficient K_s (cm·min^{-1})
		0.05 ~ 0.01	< 0.01	< 0.001			
TA1	Luochuan	11.47	49.29	11.30	3.0	46.0	0.0136
TA2	Xiamanshuitan	39.83	37.60	4.45	27.6	49.8	0.0079
TA3	Xicao	33.14	33.42	9.70	31.9	53.0	0.0048

Table 1. Soil hydraulic parameters in the test areas.

(Fig. 6a). S was then substituted into Eq. (14), resulting in s_f = 23.9 cm. The calculation process of S and s_f of the other test areas was the same as that of test area No.1. Figure 6 shows the fitting curve of soil infiltration rate at each test point. The s_f of test areas No. 2 and No. 3 were calculated to be 674.3 cm and 290.3 cm, respectively.

The calculated s_f of each test area was inserted into Eq. (19), which allowed calculation of the wetting front depth at different infiltration times of each test area. Figures 7, 8 and 9 show the infiltration depth and relative error calculated by different methods. The relative error was calculated as follows:$\Delta = \left|\frac{I_{measured} - I_{calculated}}{I_{measured}}\right|$. Relative errors Δ closer to 0 indicate higher calculation accuracy. The wetting front infiltration depth calculated using the MLGA model established in the present study was more consistent with the measured results, indicating that the MLGA model is reliable.

For test area No. 1, the relative errors between the wetting front infiltration depth calculated by the Kostiakov model and the measured data at different infiltration times were 19.24%, 17.0%, 14.21%, 13.27% and 13.61%, respectively. The relative errors of the MLGA model were 5.07%, 4.89%, 4.67%, 3.37% and 2.05%, respectively (Fig. 7(b)). The average errors of the Kostiakov model and MLGA model are 15.46% and 4.01%, respectively, and the minimum error rates were 19.24% and 2.05%, respectively.

At test area No. 2, when the infiltration time was 17, 38, 50, and 70 min, the relative errors between the infiltration depth calculated by the Kostiakov model and the measured data were 36.40%, 15.26%, 22.94%, and 19.42%, respectively, whereas the relative errors of the LGAM model were 7.01%, 6.52%, 5.26%, and 11.03%,

Area No.	Test area	Infiltration time t (min)	Cumulative infiltration I (cm)
TA1	Luochuan	10	1.76
		22	2.79
		30	3.28
		40	3.75
		51	4.23
		60	4.66
		68	4.94
TA2	Xiamanshuitan	10	2.88
		19	5.06
		30	7.29
		38	9.07
		50	11.25
		66	13.96
TA3	Xicao	20	2.44
		40	3.76
		60	4.95
		80	6.08
		155	10.14
		200	12.48

Table 2. Measured cumulative infiltration of the test areas.

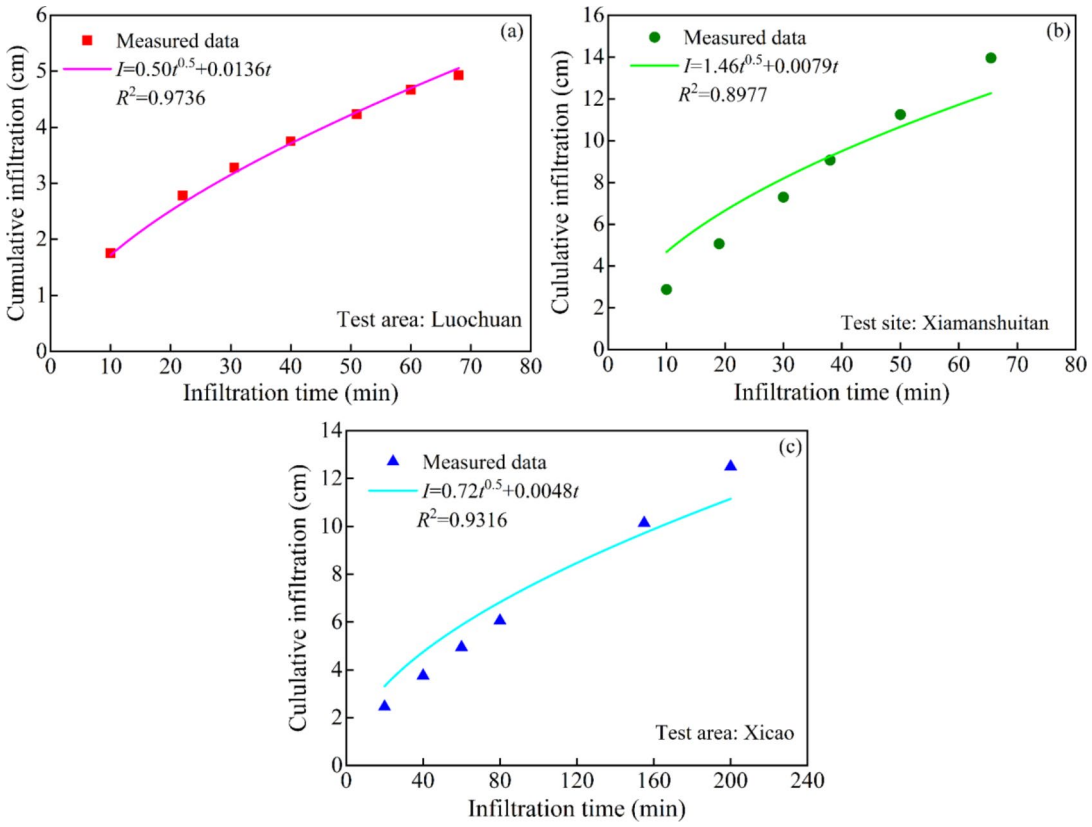

Fig. 6. Fitting curves of the infiltration rates of different test areas (test areas No. 1 (**a**), No. 2 (**b**), and No. 3 (**c**)).

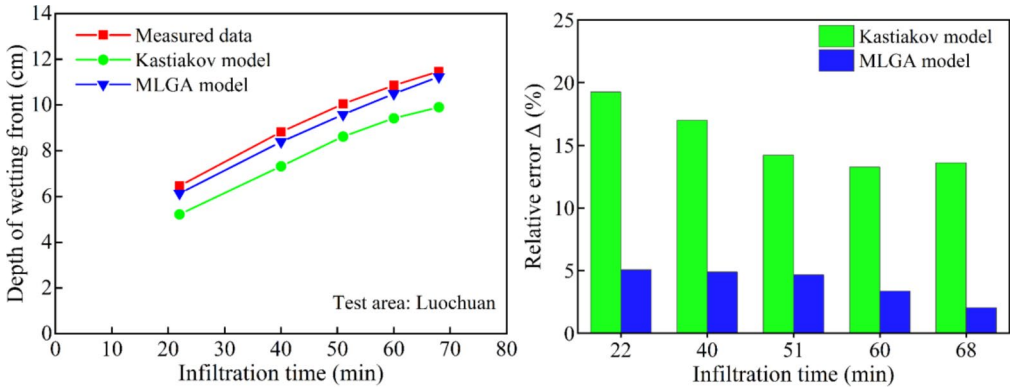

Fig. 7. Infiltration depth analysis of test area No. 1. (**a**) Comparison of measured data and calculated results. (**b**) Relative error.

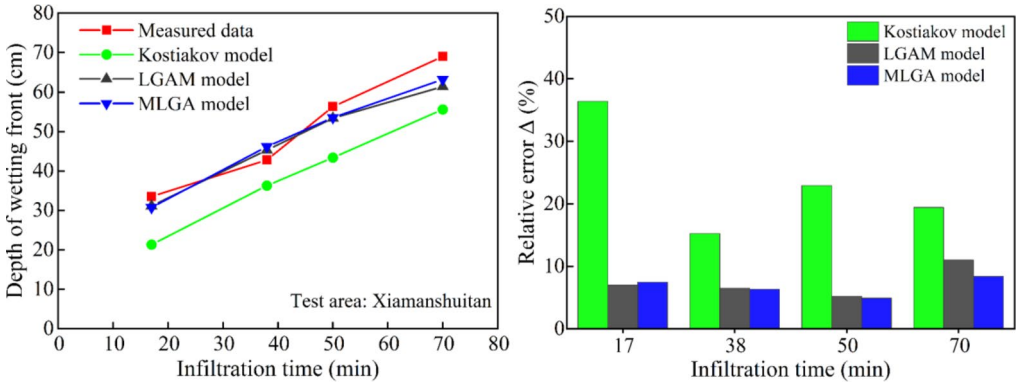

Fig. 8. Infiltration depth analysis of test area No. 2. (**a**) Comparison of measured data and calculated results. (**b**) Relative error.

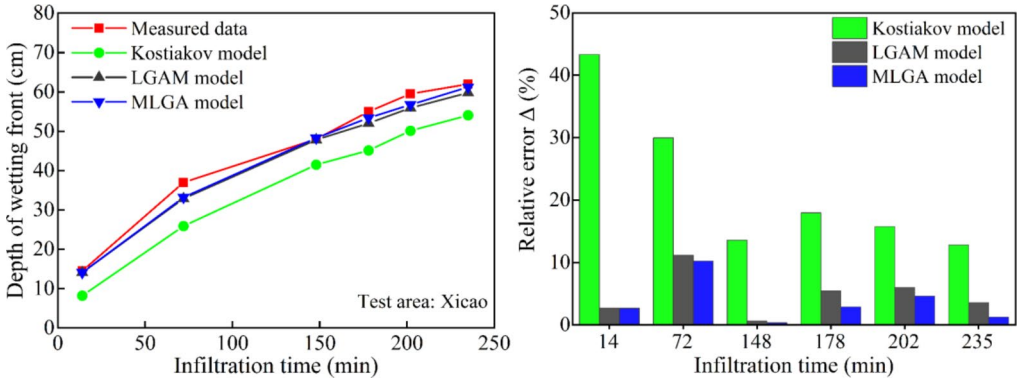

Fig. 9. Infiltration depth analysis of test area No. 3. (**a**) Comparison of measured data and calculated results. (**b**) Relative error.

respectively. The relative errors of the MLGA model were 7.34%, 6.28%, 4.91%, and 8.39%, respectively (Fig. 8(b)). Further, the average errors of the Kostiakov model, LGAM model, and MLGA model were 23.50%, 7.46%, and 6.73%, while the maximum errors were 36.40%, 11.03%, and 8.39%, respectively.

As for test area 3, when the infiltration time increased from 14 min to 235 min, the relative errors between the infiltration depth calculated by the Kostiakov model and the measured data were 43.32%, 29.98%, 13.57%, 17.96%, 15.76% and 12.81%, respectively. The relative errors of LGAM model were 2.66%, 11.15%, 5.98%, 5.43%, 6.03% and 3.59%, respectively. The relative errors of MLGA model were 2.69%, 10.24%, 3.58%, 2.89%, 4.63% and 1.27%, respectively (Fig. 9(b)). The average errors of the three models were 22.40% (Kostiakov model), 5.81%

(LGAM model) and 4.22% (MLGA model), and the corresponding minimum errors were 12.81%, 3.59% and 1.27%.

It is also necessary to explain that the wetting front infiltration rate slows down with infiltration time increases (Figs. 7(a), 8(a), and 9(a)). In response to this phenomenon, Tu et al.[44], Mei et al.[45], and Ma et al.[46] reached the same conclusion, indicating that the basic assumptions adopted by the MLGA model did not change the basic properties of the infiltration model and could describe the infiltration characteristics. In summary, compared with other existing models, the calculated results of the MLGA model were the closest to the measured data. Thus, the calculation model is accurate and effective, and it has good adaptability in loess areas.

Although the calculation accuracy of the MLGA model was high, there was still some deviation from the measured data, which may be caused by the special complex soil conditions of loess areas[3,47,48]. Because loess has the characteristics of vertical joint development and large pore structure, water can infiltrate rapidly along joints and large pores[49,50]. In addition, the content of calcium and soluble salt in loess is high. Under the condition of water infiltration, the cementing material between particles is continuously dissolved, and the cementing structure is destroyed. As a result, soil particles are eroded and transported, resulting in changes in pore structure and further development and extension of connected pores[51,52]. However, the influence of the above factors was not considered in the MLGA model, indicating that the calculation results were conservative. In general, the infiltration depth calculated by the MLGA model was close to the measured value, which is suitable for infiltration analysis of loess sites. In addition, the calculation results of the MLGA model were similar to those of the LGAM model. These models will be discussed in further detail later.

Parameter analysis

The influences of saturated permeability coefficient K_s, initial water content θ_i, saturated water content θ_s, and matrix suction s_f on the infiltration depth reflected by the model in the present study were investigated through parameter analysis. The aim was to quantify the influence of each parameter on the depth of the wetting front, screen out the parameters that need to be accurately calibrated, and enhance the accuracy and efficiency of the model. Test area No. 2 was taken as the example of the calculation, and its soil properties parameters were taken as the basic parameters for parametric analysis by changing a single variable. Four levels were selected for each parameter, and their influence on infiltration depth was compared and analyzed.

Saturation permeability coefficient *Ks*

When keeping other parameters unchanged, the saturated permeability coefficient K_s was utilized as the variable. When K_s = 0.004, 0.016, 0.032, and 0.05 cm·min^{-1}, the infiltration depth of the wetting front was calculated, and the influence of K_s on infiltration depth was analyzed. Figure 10 illustrates the comparison of the infiltration depth for different saturation permeability coefficients. The depth of infiltration gradually increased with the gradual increase of the saturation permeability coefficient at the same infiltration time point. For example, when the infiltration time was 70 min, the calculated infiltration depth under K_s = 0.05 cm·min^{-1} was 159.33 cm, which was 3.54 times that under K_s = 0.004 cm·min^{-1}. In addition, the slope of the infiltration depth variation curve with infiltration time calculated by different saturation permeability coefficients gradually decreased with the increase of infiltration time. Considering K_s = 0.032 cm·min^{-1}, the slopes of the infiltration depth curves at different infiltration time points were 1.51, 1.23, and 0.99, respectively. Thus, these findings indicated that the permeability coefficient significantly influences the infiltration depth at the initial stage of infiltration, and the effect weakens as the infiltration duration increases.

Initial water content ϑ_i

When other parameters were kept constant, the initial water content θ_i was utilized as the variable to calculate the infiltration depth of wetting fronts at θ_i = 16%, 22%, 34%, and 40%, and the effects of θ_i on the infiltration depth were analyzed. Figure 11 shows the infiltration depth calculated using the MLGA model under four different

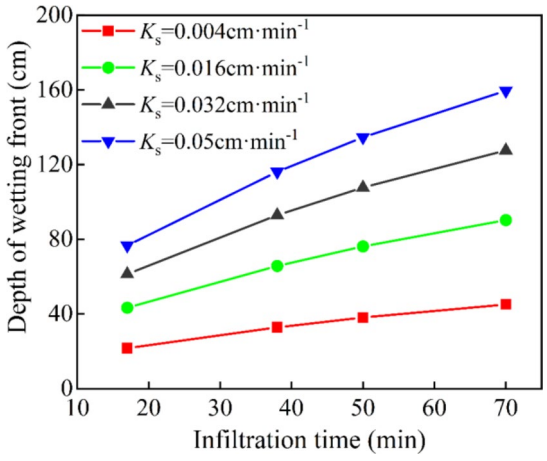

Fig. 10. Comparison of infiltration depth under different saturated permeability coefficients.

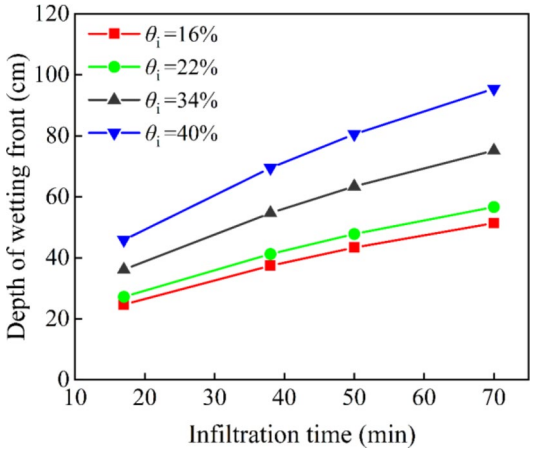

Fig. 11. Comparison of infiltration depth under different initial water content conditions.

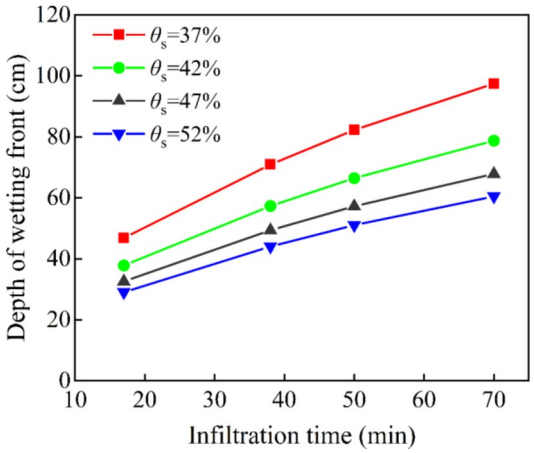

Fig. 12. Comparison of infiltration depth under different saturated water content conditions.

conditions. In general, the wetting front infiltration depth increased with the initial water content increased (Fig. 11).

Considering the infiltration time of 38 min as an example, the change in infiltration depth was 3.85 cm when the initial water content θ_i was increased from 16 to 22%. However, the difference was 14.78 cm when the initial water content θ_i increased from 34 to 40%. These results demonstrated that the change in infiltration depth is not significant under the same water content increase when the initial water content is at a low level. When the initial water content is at a high level, the increase in water content will considerably impact the infiltration depth. Moreover, the difference in infiltration depth under different initial water content also increases gradually as the infiltration time increases, indicating that the influence of initial water content on the infiltration depth gradually increases with the increase of infiltration time.

Saturated water content ϑ_s

While keeping the other parameters constant, the saturated water content θ_s was utilized as the variable. The infiltration depth of the wetting front was calculated when θ_s was 37%, 42%, 47%, and 52%, and the influence of θ_s on infiltration depth was analyzed. Figure 12 compares infiltration depth calculated by the MLGA model under different saturated water content conditions. As in Fig. 12, the depth of infiltration gradually decreased with the saturated water content increased. In particular, the distance between the curves of infiltration depth over time under different saturated water content conditions was not equal under the condition of the same increase in water content, and the distance increased gradually with the passage of infiltration time. For example, when the infiltration time was 50 min, the four curves were subtracted from high to low, and the differences were 15.79 cm, 9.20 cm, and 6.21 cm. When the infiltration time was 70 min, the differences were 18.72 cm, 10.91 cm and 7.34 cm. These findings indicated that the influence of saturated water content on the infiltration depth increases with the increase of infiltration time.

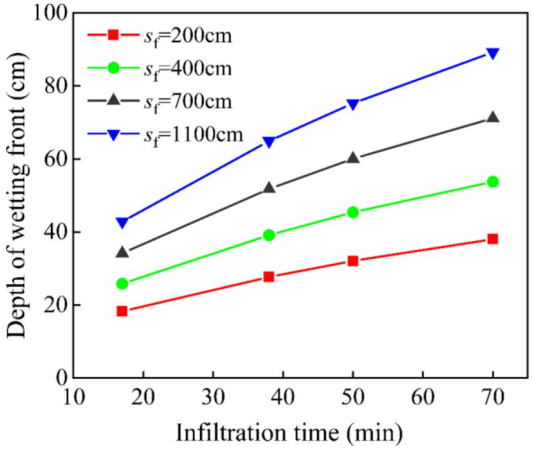

Fig. 13. Comparison of infiltration depth under different matric suction conditions.

Levels	Range of S values	Sensitivity characterization
I	$\|S\|\geq 1$	High sensitivity parameter
II	$0.2\leq\|S\|<1$	Sensitivity parameter
III	$0.05\leq\|S\|<0.2$	Medium sensitivity parameter
IV	$0\leq\|S\|<0.05$	Insensitivity parameter

Table 3. Parameter sensitivity grading table.

Matrix suction s_f

By maintaining the other parameters constant, matrix suction s_f was utilized the variable. The infiltration depth of the wetting front was calculated when s_f = 200, 400, 700 and 1100 cm, and the influence of s_f on infiltration depth was analyzed. Figure 13 shows the comparison of the depth of infiltration calculated by this model under four conditions. The depth of infiltration increased with the increase of matrix suction (Fig. 13). As an example, when the infiltration time was 70 min, the infiltration depth was 38.03 cm under s_f = 200 cm, which was 42.6% of the value under s_f = 1100 cm. Under different matrix suction conditions, the slopes of the four infiltration depth time versus time curves gradually decreased, showing the same trend. These results indicated that the sensitivity of infiltration depth to matrix suction decreases with time.

Sensitivity analysis of different parameters

Sensitivity analysis was performed using the modified Morris method to analyze the influence of saturated permeability coefficient K_s, initial water content θ_i, saturated water content θ_s, and matrix suction s_f on infiltration depth. When considering the soil parameters of test area No. 2 as the basic parameters, each parameter was disturbed up and down with a step size of 10%. Based on previous studies[53], a 20% increase or decrease in the range of variation of each parameter is reasonable. Sensitivity index S is calculated as follows:

$$S = \sum_{i=1}^{N-1} \left[\frac{(Y_{i+1} - Y_i)/Y_0}{(P_{i+1} - P_i)/P_0} \right] / (N-1) \tag{20}$$

where Y_i and P_i are the output value and the adjustment ratio of the parameters to the initial parameter value for the i^{th} run, respectively; Y_{i+1} and P_{i+1} are the output value and the adjustment ratio of the parameters to the initial parameter value for the $i+1$th run, respectively; and N is the number of model runs.

The sensitivity grades of the parameters are shown in Table 3.

Figure 14 shows the calculated values of infiltration depth and the sensitivity of each factor to the infiltration depth when the infiltration time is 70 min. The sensitivity order of the impact of disturbance on the infiltration depth of the four soil parameters was $\theta_s > \theta_i > s_f > K_s$. The sensitivity levels of all four parameters were II, except for saturation water content, which had a sensitivity level of I. Therefore, the accuracy of θ_s is important when using this model to calculate the infiltration depth. Furthermore, θ_i, s_f, and K_s disturbance were positively correlated with infiltration depth, while θ_s disturbance was negatively correlated with infiltration depth (Fig. 14).

Discussion

Comparison with other models

The present study demonstrated that the infiltration depth values calculated by the MLGA model and the LGAM model were close to the measured results, indicating that both models have certain adaptability to the prediction

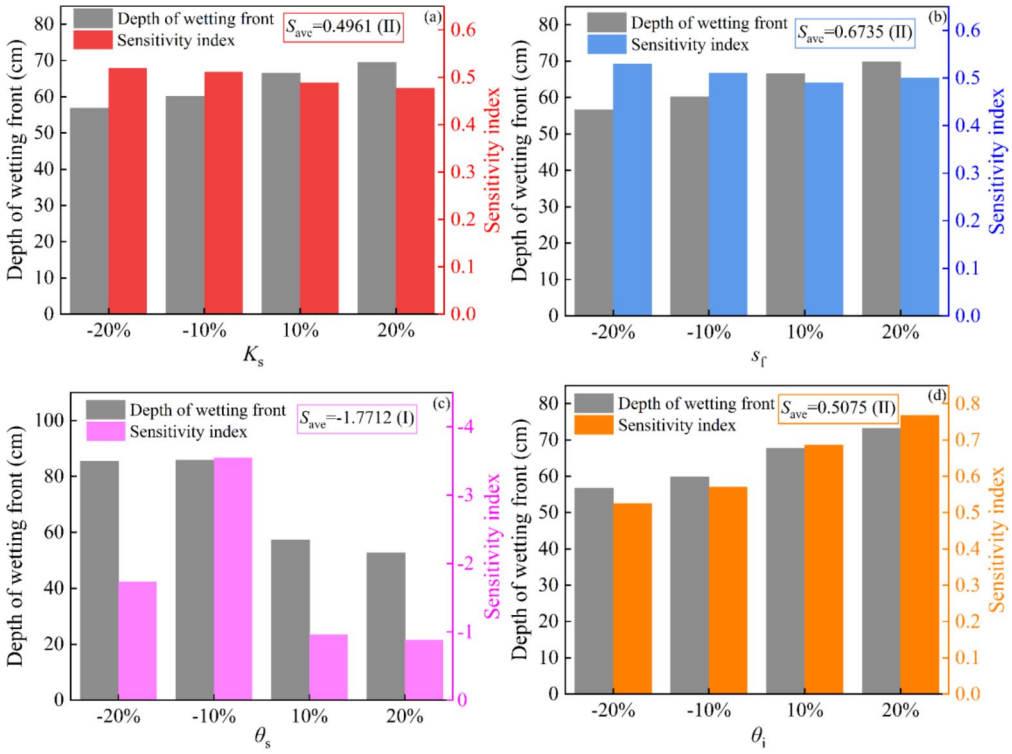

Fig. 14. Effect of soil parameter disturbance on the depth of wetting front on the basis of K_s, s_f, θ_s, and θ_i (a-d, respectively).

of infiltration depth in loess areas. However, the MLGA model was more reasonable than the LGAM model in describing the physical process of infiltration. According to the derivation process of the LGAM model, the LGAM model assumes that the permeability coefficient of the wet layer is $K \leq K_s$, and the other assumptions are consistent with the basic assumptions of the model. Moreover, the LGAM model obtains model parameters through the correlation between the Philip model and the GA model. Thus, the two models have the same physical basis.

The equation of the LGAM model to calculate the cumulative infiltration is the same as Eq. (4) in the present study. Infiltration rate i is expressed as follows:

$$i = \frac{dL}{dt} = K\frac{0.5L + h_0 + s_f}{0.5L} \tag{21}$$

By combining Eqs. (4) and (21), the equation is written as follows:

$$\frac{dL}{dt} = \frac{16K}{(4+\pi)(\theta_s - \theta_i)}\left[\frac{0.5L + h_0 + s_f}{L}\right] \tag{22}$$

When the infiltration time is small, 0.5 L can be negligible compared with (s_f+h_0).

The infiltration depth L is written as follows:

$$L = \sqrt{\frac{32K(h_0 + s_f)t}{(4+\pi)(\theta_s - \theta_i)}} \tag{23}$$

The above analysis indicates that the LGAM model takes into account the change of permeability coefficient K with depth in the process of infiltration, which is an advanced feature. However, the LGAM model ignores the saturation depth of 0.5 L at the initial stage of infiltration, and its derivation process is not reasonable and is inconsistent with the actual situation of water infiltration in loess areas. Although the actual situation in which the permeability coefficient decreases along the depth is not fully considered in the MLGA model, the infiltration equation that aligns with the actual water infiltration law is deduced, representing the advancement of the model in the present study.

The results from Sect. 4.1 and 4.5 indicated that the influence of infiltration depth on the permeability coefficient decreases with time, and infiltration depth is the least sensitive to the permeability coefficient. Therefore, although there are some limitations in calculating the saturated permeability coefficient, the accuracy is satisfactory (Sect. 3). In summary, the MLGA model considers the water infiltration process more comprehensively than the LGAM model and has certain advantages.

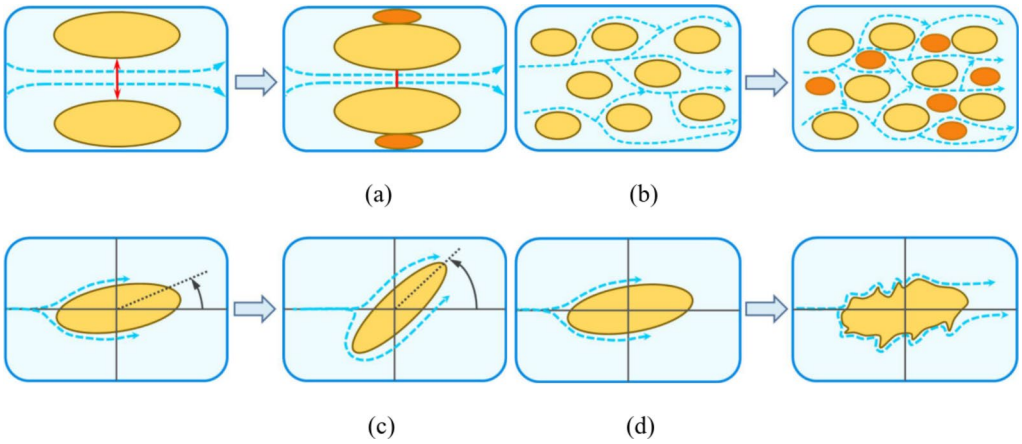

Fig. 15. Mechanisms affecting saturated permeability coefficients, including width, bending degree, angle, and roughness (a-d, respectively).

Influence mechanism of key parameters

Section 4 described the sensitivity analysis of the four main model parameters affecting the water infiltration depth. The influence of main model parameters on infiltration depth was analyzed from qualitative and quantitative aspects. However, the mechanism of influence of each parameter on infiltration depth was not the same.

As an essential parameter to characterize the permeability of soil, saturated permeability coefficient *K*s is the basis for investigating the water infiltration process of soil and has a remarkable impact on the water infiltration process. The physical meaning of the saturated permeability coefficient is the ability of the soil allowing water to pass when saturated, that is, the greater the saturated permeability coefficient of the soil, the greater the water infiltration rate. Soil is affected by physical weathering and chemical erosion, and there are differences in microstructure morphology and distribution characteristics, which affect the water passage process, manifested as different permeability coefficients[54]. In general, loose soil has a large saturated permeability coefficient because the number of soil pores is large, the connectivity is strong, and water can easily pass through.

Previous studies have suggested that the pore channel is the main factor affecting the permeability coefficient of soil, and the shape and distribution characteristics of soil particles influence the pore channel[55,56]. With respect to geometric morphology, scholars have characterized the shape and surface characteristics of soil particles by ellipticity and roughness. Moreover, the size, area content, and anisotropy of soil particles are described by gradation, void ratio, and long axis dip angle. The soil gradation and porosity directly affect the 'width' and 'bending degree' of the infiltration channel, thereby affecting the permeability of the soil.

With the increase of fine particle content and the decrease of porosity in soil, the number of soil particles in the same unit area increased, which led to an increased turning point of the infiltration channel and reduced relative distance between soil particles (Fig. 15a-b). An increase in the turning point of the infiltration channel indicates that the 'bending degree' of the channel increases, and a reduction in the relative distance leads to a decrease in the 'width' of the channel. These changes increase the infiltration resistance and reduce the permeability coefficient of the soil. The particle ellipticity and the long axis inclination angle affect the 'angle' and 'length' of the inflection point of the infiltration channel. When the water encounters long particles that are not parallel to the infiltration direction, as the ellipticity and the long axis inclination angle increase, the 'angle' and 'length' of the inflection point of the infiltration channel increase, resulting in an increase in resistance and ultimately a decrease in the saturated permeability coefficient (Fig. 15c). For soils with high roughness, when water permeates along the surface of particles, greater flow resistance is generated, resulting in a lower soil permeability coefficient (Fig. 15d).

As a key parameter to describe the initial conditions of infiltration, the initial water content is also an essential factor in characterizing the infiltration capacity of soil. In general, the infiltration rate increases with the initial water content. Within the same infiltration time, higher initial water contents result in greater infiltration depths due to the limited water holding capacity of the soil. When the initial water content of the same soil increases, the amount of water absorbed during the infiltration process decreases accordingly, which is conducive to the continuous downward development of the wetting front.

In addition, saturated water content significantly impacts the rate and depth of infiltration. Specifically, the infiltration rate decreases with increasing saturated water content under the same soil type. Therefore, under the condition of constant initial water content, larger saturated water contents result in smaller infiltration depths when the infiltration time is the same. Increasing the saturated water content will lead to a decrease in the number of continuous water channels inside the soil, and it is difficult for the water to migrate downward, resulting in a decrease in the infiltration rate. Moreover, increased saturated water content enhances the water holding capacity of the soil, which increases the amount of water that can be accommodated, thereby reducing the infiltration depth under the same infiltration time.

Previous studies have shown that soil water potential is the driving force of soil water infiltration, and matrix potential is an essential part of soil water potential. Therefore, matrix suction is a driving force for soil water infiltration. Because greater matrix suction results in a greater driving force of infiltration, the infiltration depth is more significant at the same infiltration time.

Future work

The present study established the MLGA model, which is suitable for ponding infiltration in loess sites. According to verification using three sets of published field measured data, the MLGA model has higher calculation accuracy compared with other models. However, further evaluation is required to determine whether the MLGA model can be directly applied to other types of soil. It is widely known that water infiltration induces changes in soil microstructure[57]; when the microstructure of the soil changes, the soil parameters also change[58]. Although the change of soil parameters affects the infiltration process [60], the soil parameters related to the MLGA model are determined values and cannot change with the development of the infiltration process. Therefore, further research is needed to develop a method to determine the dynamic change of soil parameters through the combination of macro and micro perspectives, and the calculation accuracy of the MLGA model requires additional improvement. These deficiencies will be the main focus of future work.

Conclusions

The classical GA infiltration model assumes that the soil is completely saturated within the infiltration depth, ignoring the actual unsaturated layer in the infiltration process. In the present study, the characteristics of the water profile change during infiltration were fully considered, and the MLGA model suitable for water infiltration in loess sites was established. The MLGA model was verified using published experimental data. Furthermore, sensitivity analysis of the main parameters of the MLGA model was performed, and the influence mechanism of each parameter on the infiltration depth was discussed. The main conclusions are as follows:

(1) Based on the assumption of saturated-unsaturated stratification in the infiltration depth, the MLGA model reflects the variation characteristics of the water profile in the infiltration process, using Darcy 's law and the continuity equation. Considering that the Philip model and the GA model have the same physical basis, the expression of matrix suction is obtained by combining the internal relationship between the infiltration rate and cumulative infiltration of the two models. Noteworthy, the MLGA model has a reliable theoretical basis, strict derivation process, and can reflect the actual water infiltration process comprehensively and accurately, and has certain advantages.

(2) The effectiveness of the MLGA model was validated by comparing with an existing infiltration model and three sets of field measured infiltration data. The maximum relative error of the MLGA model is less than 10%, and the average relative error is 5.54%, indicating that the MLGA model has high computational accuracy. Further, the average error of the MLGA model is 24.47% of the Kostiakov model and 80.42% of the LGAM model.

(3) The key parameters of the MLGA model, namely, saturated permeability coefficient K_s, initial water content θ_i, saturated water content θ_s, and matrix suction s_f, were analyzed by the single-factor disturbance method. The influence of each parameter on infiltration depth was summarized, and the sensitivity of each parameter was quantitatively described. The sensitivity of the four parameters to the infiltration depth is $\theta_s > \theta_i > s_f > K_s$. Importantly, the accuracy of high sensitivity parameters should be ensured when the MLGA model is used for calculation. The influence mechanism of each parameter on water infiltration is analyzed finally.

Data availability

The data sets supporting the results of this article are included within the article and its additional files. Data sets generated during the current study are available from the corresponding author on reasonable request.

Received: 25 June 2024; Accepted: 8 January 2025
Published online: 11 January 2025

References

1. Rogers, C. D. F., Dijkstra, T. A. & Smalley, I. J. Hydroconsolidation and subsidence of loess: studies from China, Russia, North America and Europe: in memory of Jan Sajgalik. *Eng. Geol.* **37**(2), 83–113 (1994).
2. Liu, Z. et al. Collapsibility, composition, and microstructure of loess in China. *Can. Geotech. J.* **53**(4), 673–686 (2016).
3. Zhuang, J., Peng, J. & Zhu, Y. Study of the effects of clay content on loess slope failure mode and loess strength. *Bull. Eng. Geol. Environ.* **80**, 1999–2009 (2021).
4. Luo, H., Wu, F., Chang, J. & Xu, J. Microstructural constraints on geotechnical properties of Malan Loess: a case study from Zhaojiaan landslide in Shaanxi province, China. *Eng. Geol.* **236**, 60–69 (2018).
5. Xie, Q. et al. Strength behaviors of undisturbed Malan loess under rainfall leaching in Yan'an area, China. *Bull. Eng. Geol. Environ.* **82**(2), 53 (2023).
6. Sun, P., Peng, J., Chen, L., Lu, Q. & Igwe, O. An experimental study of the mechanical characteristics of fractured loess in western China. *Bull. Eng. Geol. Environ.* **75**, 1639–1647 (2016).
7. Meng, X., Liao, H. & Zhang, J. Research on the collapsibility of loess after water immersion. *Nat. Hazards* **109**, 303–328 (2021).
8. Wang, L., Shao, S. & She, F. A new method for evaluating loess collapsibility and its application. *Eng. Geol.* **264**, 105376 (2020).
9. Wen, X. et al. Effects of rainwater infiltration in low impact development facilities on adjacent municipal roads in collapsible loess. *Bull. Eng. Geol. Environ.* **81**(1), 25 (2022).
10. Mishra, S. K., Kumar, S. R. & Singh, V. P. Calibration and validation of a general infiltration model. *Hydrol. Process.* **13**(11), 1691–1718 (1999).

11. Al-Janabi, A. M. S., Ghazali, H., Yusuf, B. & A., & Modified models for better prediction of infiltration rates in trapezoidal permeable stormwater channels. *Hydrolog Sci. J.* **64** (15), 1918–1931 (2019).
12. Kostiakov, A. N. On the dynamics of the coefficient of water-percolation in soils and on the necessity of studying it from a dynamic point of view for purposes of amelioration. *Trans. 6th Cong Int. Soil. Sci. Russian Part. A*, 17–21 (1932).
13. Zheng, Y. et al. Slope Stability Analysis under Heavy Rainfall conditions based on a modified green-ampt model. *Water Resour. Manag* **38**(7), 2627–2646 (2024).
14. Richards, L. A. Capillary conduction of liquids through porous mediums. *Physics* **1**(5), 318–333 (1931).
15. Green, W. H. & Ampt, G. A. Study on soil physics: I. Flow of air and water through soils. *J. Agri Sci.* **4**, 1–24 (1911).
16. Arampatzis, G. et al. Estimation of unsaturated flow in layered soils with the finite control volume method. *Irrig. Drain.* **50**(4), 349–358 (2001).
17. Rao, M. D., Raghuwanshi, N. S. & Singh, R. Development of a physically based 1D-infiltration model for irrigated soils. *Agr Water Manage.* **85**(1–2), 165–174 (2006).
18. Liu, G., Li, S. & Wang, J. New Green-Ampt model based on fractional derivative and its application in 3D slope stability analysis. *J. Hydrol.* **603**, 127084 (2021).
19. Li, S. H., Cui, P., Cheng, P. & Wu, L. Z. Modified green–ampt model considering vegetation root effect and redistribution characteristics for slope stability analysis. *Water Resour. Manag* **36** (7), 2395–2410 (2022).
20. Kale, R. V. & Sahoo, B. Green-Ampt infiltration models for varied field conditions: a re*visit*. *Water Resour. Manag.* **25**, 3505–3536 (2011).
21. Deng, P. & Zhu, J. Analysis of effective green–ampt hydraulic parameters for vertically layered soils. *J. Hydrol.* **538**, 705–712 (2016).
22. Mein, R. G. & Larson, C. L. Modeling infiltration during a steady rain. *Water Resour. Res.* **9**(2), 384–394 (1973).
23. Chu, S. T. Infiltration during an unsteady rain. *Water Resour. Res.* **14**(3), 461–466 (1978).
24. Liu, J., Zhang, J. & Feng, J. Green–ampt model for layered soils with nonuniform initial water content under unsteady infiltration. *Soil. Sci. Soc. Am. J.* **72**(4), 1041–1047 (2008).
25. Cho, S. E. Prediction of shallow landslide by surficial stability analysis considering rainfall infiltration. *Eng. Geol.* **231**, 126–138 (2017).
26. Yao, W., Li, C., Zhan, H. & Zeng, J. Time-dependent slope stability during intense rainfall with stratified soil water content. *Bull. Eng. Geol. Environ.* **78**, 4805–4819 (2019).
27. Dou, H. Q., Han, T. C., Gong, X. N. & Zhang, J. Probabilistic slope stability analysis considering the variability of hydraulic conductivity under rainfall infiltration–redistribution conditions. *Eng. Geol.* **183**, 1–13 (2014).
28. Ma, Y., Feng, S., Su, D., Gao, G. & Huo, Z. Modeling water infiltration in a large layered soil column with a modified green–ampt model and HYDRUS-1D. *Compu Electron. Agr* **71**, S40–S47 (2010).
29. Tsai, Y. Z., Liu, Y. T., Wang, Y. L., Chang, L. C. & Hsu, S. Y. Effects of the grain size on dynamic capillary pressure and the modified green–ampt model for infiltration. *Geofluids* **2018** (1), 8946948 (2018).
30. Kang, S. et al. A modified green-ampt infiltration model for muddy water. *J. Hydrol.* **629**, 130606 (2024).
31. Zha, F. et al. Modification of Green-Ampt model based on multi-stage characteristics of soil water infiltration. *Hydrolog Sci. J.* **69**(12), 1652–1662 (2024).
32. Wang, W. Y., Wang, Z. R., Wang, Q. J. & Zhang, J. F. Improvement and evaluation of the Green-Ampt model in loess soil. *J. Hydraul Eng.* **35**, 30–35 (2003).
33. Peng, Z. Y., Huang, J. S., Wu, J. W. & Guo, H. Modification of Green-Ampt model based on the stratification hypothesis. *Adv. Water Sci.* **23**(1), 59–66 (2012).
34. Wen, X., Hu, Z. P., Zhang, X., Chai, S. B. & Lv, X. B. Modified infiltration model for saturated-unsaturated loess based on Green-Ampt model and its parametric study. *Rock. Soil. Mech.* **41**(6), 1991–2000 (2020).
35. Risse, L. M., Nearing, M. A. & Savabi, M. R. Determining the Green-Ampt effective hydraulic conductivity from rainfall-runoff data for the WEPP model. *Trans. ASAE* **37**(2), 411–418 (1994).
36. Gowdish, L. & Muñoz-Carpena, R. An improved green–ampt infiltration and redistribution method for uneven multistorm series. *Vadose Zone J.* **8**(2), 470–479 (2009).
37. Van den Putte, A. et al. Estimating the parameters of the green–ampt infiltration equation from rainfall simulation data: why simpler is better. *J. Hydrol.* **476**, 332–344 (2013).
38. Hillel, D. & Gardner, W. R. Transient infiltration into crust-topped profiles. *Soil. Sci.* **109**(2), 69–76 (1970).
39. Barrera, D. & Masuelli, S. An extension of the Green-Ampt model to decreasing flooding depth conditions with efficient dimensionless parametric solution. *Hydrolog Sci. J.* **56**(5), 824–833 (2011).
40. Zhang, Q., Chen, W. & Kong, Y. Modification and discussion of the Green-Ampt model for an evolving wetting profile. *Hydrolog Sci. J.* **65**(12), 2072–2082 (2020).
41. Philip, J. R. The theory of infiltration: 1. The infiltration equation and its solution. *Soil. Sci.* **83**(5), 345–358 (1957).
42. Regalado, C. M., Ritter, A., Alvarez-Benedi, J. & Muñoz-Carpena, R. Simplified method to estimate the green–ampt wetting front suction and soil sorptivity with the philip–dunne falling-head permeameter. *Vadose Zone J.* **4**(2), 291–299 (2005).
43. Liu, J. L., Ma, X. Y. & Zhang, Z. H. Applicability of explicit functions on cumulative infiltration of Green-Ampt model under different conditions. *J. Basic. Sci. Eng.* **18**(1), 11–19 (2010).
44. Tu, X. B., Kwong, A. K. L., Dai, F. C., Tham, L. G. & Min, H. Field monitoring of rainfall infiltration in a loess slope and analysis of failure mechanism of rainfall-induced landslides. *Eng. Geol.* **105**(1–2), 134–150 (2009).
45. Mei, X. et al. Effect of stand origin and slope position on infiltration pattern and preferential flow on a Loess hillslope. *Land. Degrad. Dev.* **29**(5), 1353–1365 (2018).
46. Ma, J. et al. Characterization and quantitative evaluation of preferential infiltration in loess, based on a soil column field test. *Catena* **213**, 106164 (2022).
47. Peng, J., Tong, X., Wang, S. & Ma, P. Three-dimensional geological structures and sliding factors and modes of loess landslides. *Environ. Earth Sci.* **77**(19), 675 (2018).
48. Li, X. A., Wang, L., Yan, Y. L., Hong, B. & Li, L. C. Experimental study on the disintegration of loess in the Loess Plateau of China. *Bull. Eng. Geol. Environ.* **78**, 4907–4918 (2019).
49. Zhang, D., Wang, G., Luo, C., Chen, J. & Zhou, Y. A rapid loess flowslide triggered by irrigation in China. *Landslides* **6**, 55–60 (2009).
50. Xu, L. & Coop, M. R. Influence of structure on the behavior of a saturated clayey loess. *Can. Geotech. J.* **53**(6), 1026–1037 (2016).
51. Li, G. et al. Variations in strength and deformation of compacted loess exposed to wetting-drying and freeze-thaw cycles. *Cold Reg. Sci. Tech.* **151**, 159–167 (2018).
52. Hou, X. et al. Microstructure and soil-water retention behavior of compacted and intact silt loess. *Eng. Geol.* **277**, 105814 (2020).
53. Ebrahimian, H., Ghaffari, P., Ghameshlou, A. N., Tabatabaei, S. H. & Dizaj, A. A. Extensive comparison of various infiltration estimation methods for furrow irrigation under different field conditions. *Agr Water Manage.* **230**, 105960 (2020).
54. Huang, X. W., Jiang, P. P., Zhou, A. Z., Wang, W. & Tang, C. X. Prediction model for soil permeability based on fractal characteristics of particles. *Chin. J. Geotech. Eng.* **45**(9), 1907–1915 (2023).
55. Liu, Y. F. & Jeng, D. S. Pore scale study of the influence of particle geometry on soil permeability. *Adv. Water Resour.* **129**, 232–249 (2019).
56. Zhuang, J., Kong, J., Zhu, Y. & Peng, J. The structural evolution of undisturbed loess due to water infiltration. *Sci. Rep.* **14**(1), 14880 (2024).

57. Xu, P., Zhang, Q., Qian, H., Qu, W. & Li, M. Microstructure and permeability evolution of remolded loess with different dry densities under saturated seepage. *Eng. Geol.* **282**, 105875 (2021).
58. Li, P., Xie, W., Pak, R. Y. & Vanapalli, S. K. Microstructural evolution of loess soils from the Loess Plateau of China. *Catena* **173**, 276–288 (2019).

Author contributions

YZ: Investigation, Data Curation, Formal analysis, Writing - Original Draft.ZH: Conceptualization, Methodology, Project administration, Writing - Review & Editing.RW: Conceptualization, Methodology, Project administration, Writing - Review & Editing.SC: Conceptualization, Methodology, Validation.XR: Conceptualization, Investigation.YZ: Methodology, Investigation.

Funding

This research is funded by the Funding for basic research on sponge city in Fengxi New City Xixian New District (SXLHZB2017-1396), the Natural Science Foundation of Shaanxi Province (2022JQ-435) and the Fundamental Research Funds for the Central Universities (Grant No. 300102282719).

Declarations

Competing interests

The authors declare no competing interests.

Consent for publication

Written informed consent for publication was obtained from all participants.

Additional information

Correspondence and requests for materials should be addressed to Z.H.

Reprints and permissions information is available at www.nature.com/reprints.

Publisher's note Springer Nature remains neutral with regard to jurisdictional claims in published maps and institutional affiliations.